RAPID COMMUNICATION

Influence of defects in SiC (0001) on epitaxial graphene*

Guo Yu(郭 钰), Guo Li-Wei(郭丽伟)†, Lu Wei(芦 伟), Huang Jiao(黄 郊), Jia Yu-Ping(贾玉萍), Sun Wei(孙 伟), Li Zhi-Lin(李治林), and Wang Yi-Fei(王逸非)

Research & Development Center for Functional Crystals, Beijing National Laboratory for Condensed Matter Physics, Institute of Physics, Chinese Academy of Sciences, Beijing 100190, *China*

(Received 18 March 2014; revised manuscript received 8 May 2014; published online 10 June 2014)

Defects in silicon carbide (SiC) substrate are crucial to the properties of the epitaxial graphene (EG) grown on it. Here we report the effect of defects in SiC on the crystalline quality of EGs through comparative studies of the characteristics of the EGs grown on SiC (0001) substrates with different defect densities. It is found that EGs on high quality SiC possess regular steps on the surface of the SiC and there is no discernible *D* peak in its Raman spectrum. Conversely, the EG on the SiC with a high density of defects has a strong *D* peak, irregular stepped morphology and poor uniformity in graphene layer numbers. It is the defects in the SiC that are responsible for the irregular stepped morphology and lead to the small domain size in the EG.

Keywords: graphene, silicon carbide, defect

PACS: 65.40.−b, 68.35.−p **DOI:** 10.1088/1674-1056/23/8/086501

1. Introduction

Graphene is an attractive material for high-speed electronic device applications because of its extremely high carrier mobility and other intriguing properties.[1–5] Among the routes towards fabrication of graphene, thermal decomposition of semi-insulating (SI) SiC (0001) for epitaxial graphene (EG) is one of the most promising options for future large-scale integration circuit on a wafer scale[6–11] due to its compatibility with existing semiconductor processing.[5,12–14] However, up to now, the highest carrier mobility of EGs on SiC (0001) has been much smaller than that of exfoliated graphenes.[15] The existence of defects in EGs and possible additional scatterings from the buffer layer are thought to be the two major reasons responsible for the observed low carrier mobility. The defects of EG have a close relation with the morphology and dislocations of SiC (0001). The surface stepped morphology of SiC (0001) is reported to vary a lot, with step heights changing from sub-nanometres to several tens of nanometres, and terrace widths changing from sub-micrometers to several tens of micrometers,[16,17] which is believed to be caused by the SiC basal plane stacking sequence or the detailed growth conditions.[7,16–18] The hexagonal holes are also observed on the surface of SiC (0001) frequently after graphene growth,[19] which is usually explained by the insufficient migration of excess C atoms, making steps split and move along different directions.[19,20] These step edges and hexagonal holes on SiC (0001) are the scattering sources to carriers in EGs.

On the other hand, the preparation conditions are found to have a profound effect on the morphology of SiC (0001). Wang *et al.* found that the annealing rate contributed to the final stepped structure and density of hexagonal holes on SiC (0001).[7] Oleveira *et al.* observed that the step bunching could be suppressed when the initial SiC surface is composed of large steps of about 13 nm in height.[18] Luxmi *et al.* found that a higher growth temperature helps promote the migrating of excess C atoms and improves the morphology of SiC (0001), but at the same time also promotes forming step bunching on SiC (0001).[16] Up to now, the forming regular stepped morphologies and removing hexagonal holes on SiC (0001) have been still great challenges to researchers and the detailed mechanisms governing the phenomena need to be explored further.

Here we give strong evidence that the defects in SiC (0001) have a close relationship with the quality of EG grown on the locations of the defects. It is found that the defects in SiC are the essential causes of promoting step bunching and forming hexagonal holes on SiC (0001) in the thermal preparation process for EG, which leads to the small domain size in EGs. The EGs on SiC with a low defect density have a larger crystalline size than those on SiC with a high defect density. The detailed mechanism behind this phenomenon is studied and analyzed.

2. Experiment

Two semi-insulating (SI) SiC (0001) wafers, i.e., a 6H–SiC with a low dislocation density and a 4H–SiC with a little higher dislocation density, were cut into 10 mm × 10 mm pieces for usage. Their surface orientation deviating from the [0001] direction is less than 0.3°. The prepared SiC pieces were first cleaned according to the standard semiconductor wafer cleaning procedure and etched at four different tempera-

*Project supported by the National Key Basic Research Program of China (Grant No. 2011CB932700), the Knowledge Innovation Project of the Chinese Academy of Sciences (Grant No. KJCX2-YW-W22), and the National Natural Science Foundation of China (Grant Nos. 51272279 and 51072223).

†Corresponding author. E-mail: lwguo@iphy.ac.cn

© 2014 Chinese Physical Society and IOP Publishing Ltd

tures of 1100 °C, 1150 °C, and 1200 °C for 2.5 h, and 1300 °C for 3.5 h under a protecting gas ambient provided by SiC powder at a pressure of 10^{-4} Pa, to remove mechanical damage layers on SiC (0001) and to form stepped morphologies with different heights and hexagonal holes on SiC (0001). Among the etched SiC substrates, typical substrates without or with exposing defects manifested by the exposed hexagonal holes were chosen for fabricating EGs. The hexagonal holes are magnified defects in the SiC after high temperature etching. The chosen SiC pieces were placed into a graphite crucible and loaded into a high temperature furnace for graphene growth. Argon (Ar) gas was filled to 10 kPa and the temperature was raised to 1300 °C at a rate of 6 °C/min. Then the ambient pressure was lowered to about 5 Pa and kept at this pressure for 15 min–30 min for the growth of 2–3 layers of graphene on SiC (0001).[21] The morphologies of the etched SiC pieces before and after graphene growth were analyzed by an atomic force microscope (AFM) in the model Bruker Multimode-8. The crystalline quality of the EGs was characterized by Raman scattering performed on a high-resolution Raman scattering spectrometer HR800 equipped with a 532-nm laser focused to a spot of about 1 μm in diameter with a power of 1 mW. The crystalline sizes of EGs were estimated from the intensity ratios of the D peak (defect related signal) to the G peak[22,23] (I_D/I_G). The graphene layer number was estimated from the intensity ratio of the G peak to the SiC peak located at 1519 cm^{-1} ($I_G/I_{SiC(1519\ cm^{-1})}$),[24] and the intensity ratio of the G peak to the $2D$ peak (I_G/I_{2D}).[25–28] The structural uniformity of the EGs in an area of about 5 μm × 5 μm was analyzed by Raman spectrum mapping. The dynamic mechanism of graphene growth and the effects of defects in SiC on the crystalline quality and morphology of EG on SiC (0001) were analyzed and discussed. We found that the influence of defects in SiC (0001) on EG quality is serious, which reminds us that the high quality SiC substrate is a crucial prerequisite for growing high quality EGs.

3. Results and discussion

After etching under four different conditions as stated above, SiC (0001) samples undergo surface reconstruction and exhibit different morphologies. Figures 1(b) and 1(c) show the 6H–SiC and 4H–SiC (0001) surface morphologies after etching at 1100 °C respectively, and an AFM morphology of a pristine SiC piece is also given, as shown in Fig. 1(a), for comparison. It is observed that steps are all in half of a unit cell in height, 0.75 nm for 6H–SiC and 0.5 nm for 4H–SiC, in sharp contrast to the initial surfaces that are all smooth with roughness less than 0.2 nm after chemical mechanical polishing, as shown in Fig. 1(a). The terrace widths on 6H–SiC and 4H–SiC are 200 nm and 245 nm, respectively, which rely on the off-angles of the SiC (0001) substrates. The down-stair direction of the steps on etched SiC (0001) is along the off-angle direction according to the analysis and calibration using X-ray diffraction technology.

When the etching temperature is raised to 1150 °C and 1200 °C, respectively, the same stepped morphology is kept on 6H–SiC (0001), with step heights being equal to half of a unit cell of 0.75 nm, which is a relatively stable state. However, a slightly different situation happens to 4H–SiC (0001) with relatively high defect density, whose stepped morphology changes to some extent, as shown in Fig. 2(a) at 1150 °C and in Fig. 2(b) at 1200 °C. In Fig. 2(a), discontinuous terraces appear in some area located at a single terrace with a depth of 0.25 nm or 0.5 nm as marked with the circles in Fig. 2(a) and shown in the inset. Further increasing the etching temperature, the terraces become wide and step heights change from 0.25 nm to 1.0 nm, indicating step bunching forming, as shown in Fig. 2(b).

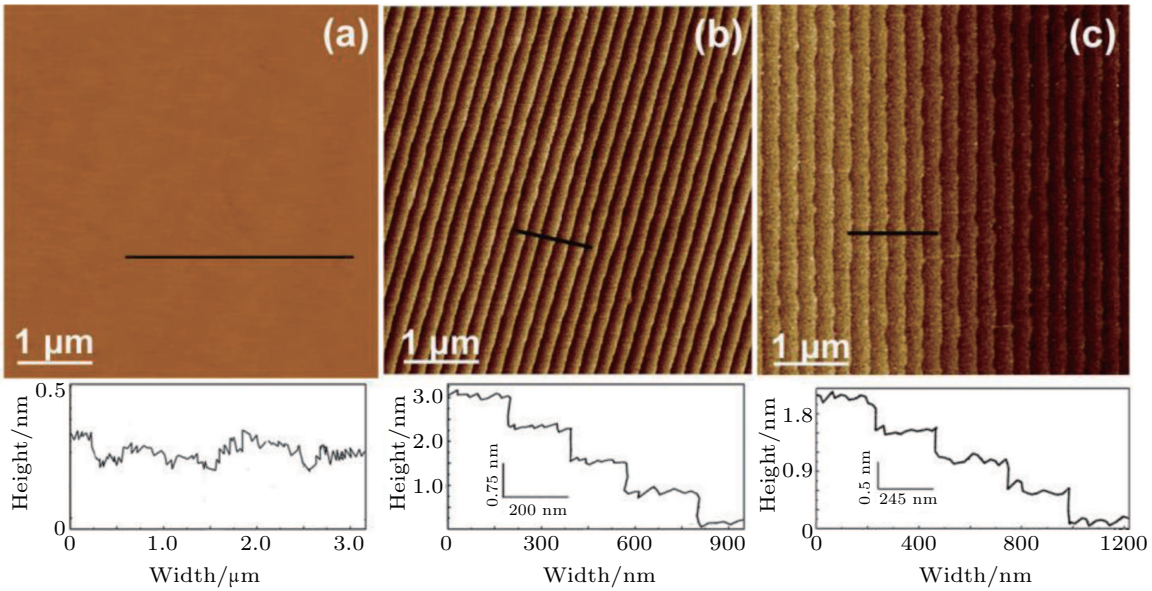


Fig. 1. (color online) AFM morphology of SiC (0001) before etching (a), and AFM morphologies of 6H–SiC (b) and 4H–SiC (c) after eaching at 1100 °C respectively. The linear profiles along the lines in the AFM images are shown in the corresponding lower panels.

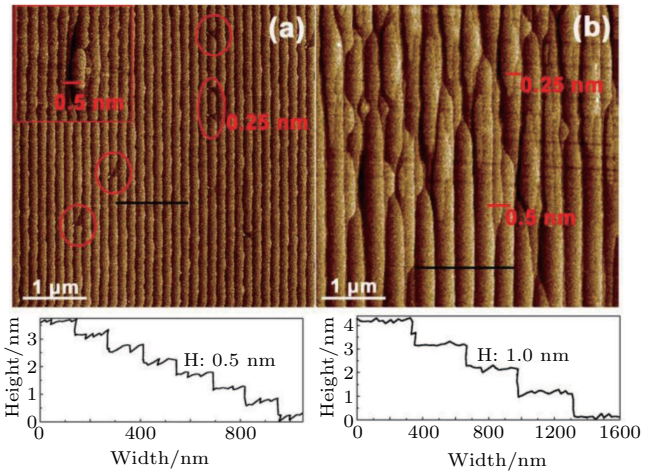


Fig. 2. (color online) AFM morphologies of 4H–SiC (0001) after etching (a) at 1150 °C and (b) at 1200 °C. The circles in panel (a) mark the defective sites with a 0.25-nm step height and the inset shows a defect developed morphology on SiC (0001) with a 0.5-nm step height. The short lines in panel (b) show the representative step heights. Linear profiles of the step morphologies along the lines in panels (a) and (b) are shown in the corresponding lower panels.

When the etching temperature is raised to 1300 °C and etching time is extended to 3.5 h, the reconstructed steps on SiC (0001) are no longer straight. Instead, spiral steps dominate on both 6H–SiC (0001) and 4H–SiC (0001) around threading screw dislocation (TSD) cores. The step heights around TSD cores are equal to half or one unit cell, as shown in Figs. 3(a)–3(c). The TSD densities are estimated to be about 1.8×10^3 cm^{-2} and 1.2×10^5 cm^{-2}, averaging counts on five different 5 μm × 5 μm areas in corresponding AFM images of the 6H–SiC and 4H–SiC respectively, which is consistent with the results estimated by a standard wet etching method.[29]

To study the morphologies of SiC (0001) after graphene epitaxy, EGs are simultaneously grown on pristine and etched SiC (0001) substrates. The AFM morphology of the EG grown on etched 6H–SiC (0001) is shown in Fig. 4(a). Those grown on etched 4H–SiC (0001) in defective and perfect regions are shown in Figs. 4(b) and 4(c) respectively. While, those grown on pristine 6H–SiC (0001) and 4H–SiC (0001) are shown in Figs. 4(d) and 4(e) respectively for comparison. The etched SiC substrates used here are annealed at 1200 °C for 2.5 h. Their AFM morphologies before graphene growth are shown in the insets of Figs. 4(a)–4(c).

In Figs. 4(a) and 4(c), it is noticed that after graphene epitaxy, most steps on etched SiC (0001) are divided into more tiny ones with heights of 0.25 nm or 0.5 nm, and the step edges have a zigzag shape. However, in Fig. 4(b), steps are non-uniform, with heights changing from 0.25 nm to 1 nm and their terraces are irregular. Meanwhile, lots of hexagonal holes are found in Fig. 4(b) with a density almost the same as that of TSDs in SiC substrate, in contrast to the few holes shown in Figs. 4(a) and 4(c). The poor morphology of Fig. 4(b) in the defective region of the SiC substrate should relate to the high defect densities existing in the 4H–SiC.

The shapes and heights of steps on the surface of SiC (0001) after graphene epitaxy on pristine SiC substrates shown in Figs. 4(d) and 4(e) are similar to those in Figs. 4(a) and 4(b), respectively. The density of hexagonal holes shown in Fig. 4(e) is almost equal to that in Fig. 4(b), except those with smaller sizes. These results shown in Figs. 4(a)–4(e) suggest that the etching process before graphene growth has no prominent influence on the morphology of SiC (0001). Therefore, it is the crystal quality of SiC substrate, specifically the defect types and densities, influences the morphologies of SiC (0001) after graphene epitaxy.

The crystalline qualities of the EGs shown in Figs. 4(a)–4(e) are analyzed by Raman scattering spectra as shown in Fig. 4(f) correspondingly, where the EGs are named EG$_{(i)}$ (i = a to e) following the alphabet letter order as indicated in Fig. 4. It is observed that there is no discernible D peak in EG$_{(a)}$, or EG$_{(c)}$ and or EG$_{(d)}$ grown on SiC (0001) with uniform stepped morphologies, no matter what crystalline prototypes the substrates have and whether they are etched or not.

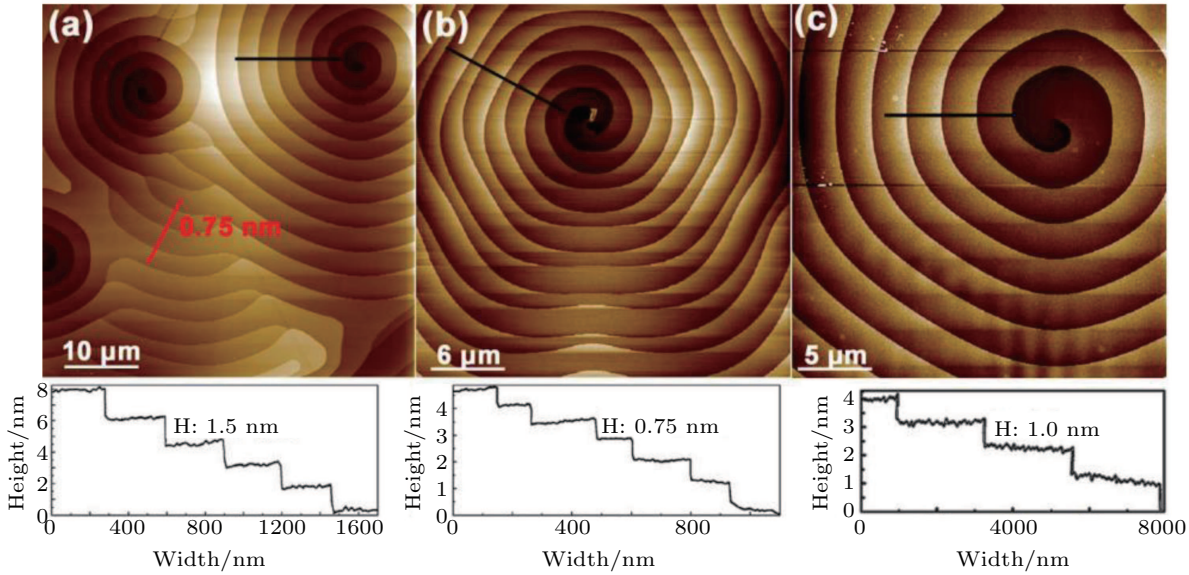


Fig. 3. (color online) AFM morphologies of TSDs exposed on 6H–SiC (0001) in panels (a) and (b), and on 4H–SiC (0001) in panel (c), after etching at 1300 °C. Linear profiles of the step morphologies along the lines are shown in the corresponding lower panels.

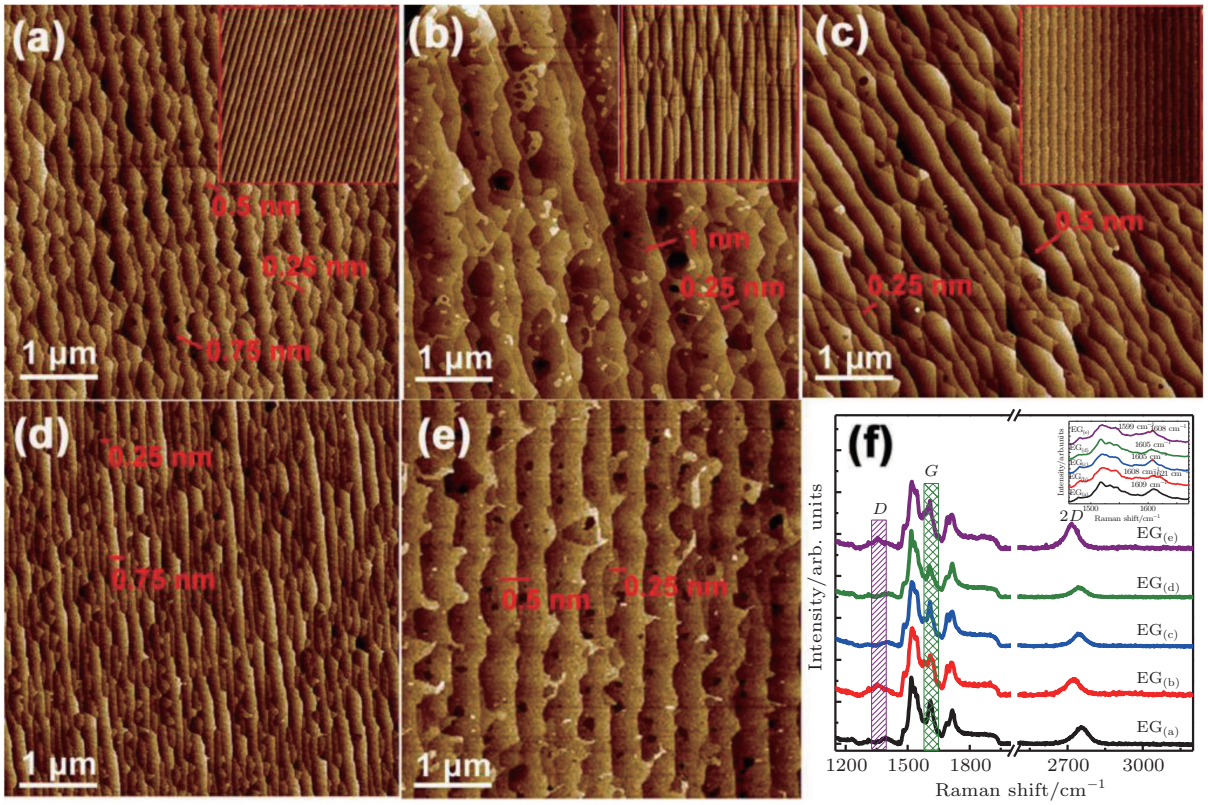


Fig. 4. (color online) AFM morphologies of the EGs on 6H–SiC (a), in the defective area of 4H–SiC (b) and in the perfect area of 4H–SiC (c) with etching, on 6H–SiC (d) and 4H–SiC (e) without etching. The insets in panels (a)–(c) show the AFM morphologies of the corresponding etched SiC substrates. (f) Raman spectra of the EGs corresponding to the images shown in panels (a)–(e), with the inset showing the magnified *G* peaks.

Yet *D* peaks are clearly present in $EG_{(b)}$ and $EG_{(e)}$ grown on SiC (0001) with a high defect density. The I_D/I_G is known to be inversely proportional to the square of crystalline sizes L_D of EG, described by the formula given by Cancado, *et al.*,[22]

$$L_D^2 = (1.8 \pm 0.5) \times 10^{-9} \lambda_L^4 (I_D/I_G)^{-1}, \qquad (1)$$

where λ_L is the excitation laser wavelength (in units of nanometer). The values of crystalline size L_D of the $EG_{(b)}$ and $EG_{(e)}$, estimated from the above formula, are about 293 nm and 360 nm, respectively, while those of $EG_{(a)}$, $EG_{(c)}$, and $EG_{(d)}$ should be much larger. Besides the *D* peak appearing in the EGs in the defective regions of the 4H–SiC substrates, their *G* peaks also split into multi-peaks as seen in the magnified *G* peaks shown in the inset of Fig. 4(f), suggesting that the domain boundaries exist on the EGs,[30] which may be induced by the irregular stepped structure in the dislocation area. The above results manifest that defect in SiC is a key factor inducing domain boundaries in EGs, and the detailed analysis will be given later.

To compare the crystal qualities of the EGs further, Raman spectrum mappings are performed on the same 5 μm × 5 μm area shown in Figs. 4(a) and 4(b), respectively, which are shown in Figs. 5(a)–5(f). The mappings of (I_D/I_G) of $EG_{(a)}$ and $EG_{(b)}$ are plotted in Figs. 5(a) and 5(b), respectively, to study their crystalline qualities, and the corresponding mappings of $I_G/I_{SiC(1519\ cm^{-1})}$ and I_G/I_{2D} are shown in Figs. 5(c)–5(f), respectively, to analyze layer number uniformity of the EGs. In Fig. 5(a), the intensity ratio of I_D/I_G is lower than 0.04, indicating a high quality of the $EG_{(a)}$ with a crystalline size larger than 3 μm estimated from Eq. (1). In Fig. 5(b), I_D/I_G changes from 0.02 to 0.53, indicating that the crystalline size of the $EG_{(b)}$ varies from about 3 μm to 288 nm. The intensity ratio $I_G/I_{SiC(1519\ cm^{-1})}$ of the $EG_{(a)}$ changes from 0.54 to 0.70 as shown in Fig. 5(c), corresponding to two to four layers of graphene films with variation less than two layers.[24] While the $I_G/I_{SiC(1519\ cm^{-1})}$ of $EG_{(b)}$ varies from 0.6 to 0.88, corresponding to three to six layers of graphene films,[24] implying that $EG_{(b)}$ is a little thicker with a slightly poorer uniformity in layer number than $EG_{(a)}$. The graphene layer numbers are also estimated according to the intensity ratio of I_G/I_{2D} to check the reliability of the deduced results.[25–28] The intensity ratios of I_G/I_{2D} change from 0.38 to 0.52 in the $EG_{(a)}$ corresponding to graphene layers two–four and from 0.45 to 0.75 in the $EG_{(b)}$ corresponding to graphene layers three–seven, respectively as shown in Figs. 5(e) and 5(f). All of these results confirm that the graphene layer numbers deduced by the two methods are consistent. It is found that the crystalline quality is poorer when the graphene layer numbers change a lot, as indicated by the $EG_{(b)}$. So the crystalline quality of EG in the defective area of the 4H–SiC (0001) is poorer than that in the perfect area on 6H–SiC (0001) should originate from the higher defect density in the SiC substrate.

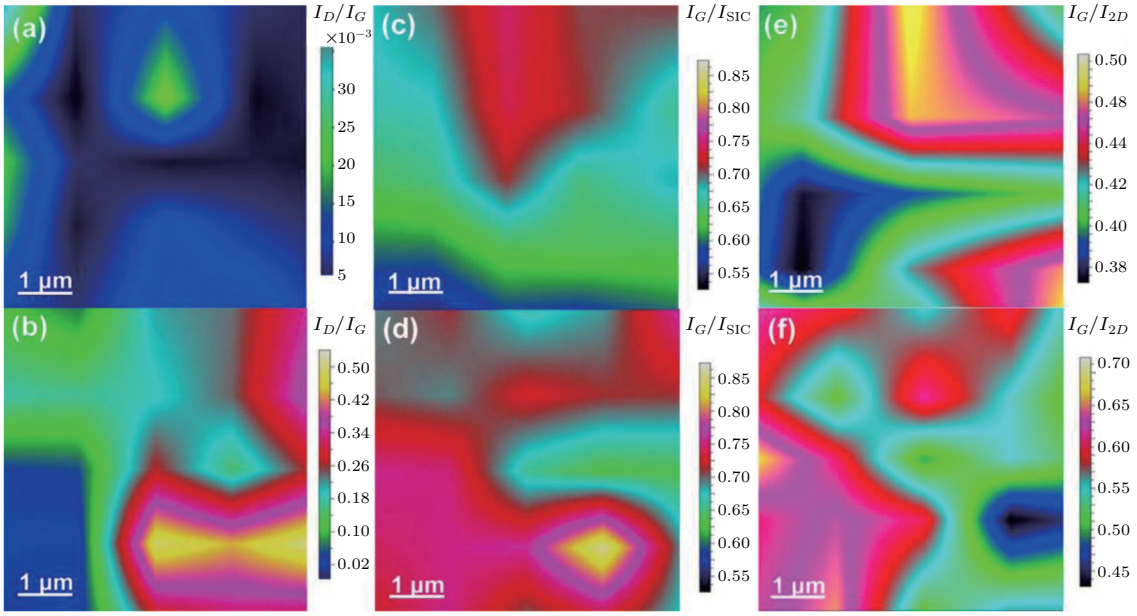


Fig. 5. (color online) Raman mappings of I_D/I_G in panels (a) and (b), $I_G/I_{\mathrm{SiC}(1519\ \mathrm{cm}^{-1})}$ in panels (c) and (d), and I_G/I_{2D} in panels (e) and (f) measured on the $\mathrm{EG}_{(a)}$ for upper mapping and on the $\mathrm{EG}_{(b)}$ for lower mapping, respectively.

A close correlation of strong *D* peaks in the EG grown on 4H–SiC with hexagonal holes after high temperature etching indicates that the defect sites in the SiC substrate may induce domain boundaries in graphene epitaxy, because the SiC crystal lattice changes its orientation on the defect sites, where the azimuth orientations of the EGs may change relatively. When the graphene islands with different azimuth orientations encounter each other, the domain boundaries form. While graphenes grown on perfect SiC (0001) should have the same azimuthal orientation governed by the crystal structure of the substrate surface,[31] so that different graphene islands connect together to form EGs with high crystalline qualities. The features of graphene grown on the defective site and in the perfect crystalline area of SiC (0001) are compared and analyzed. The AFM morphology of EGs grown on a TSD site is shown in Fig. 6(a), where the initially etched SiC substrate with the same size is shown in its inset and the corresponding Raman spectra are shown in Fig. 6(b). It is observed that the TSD core is enlarged into hexagonal holes due to the larger stress and the preferable decomposition of SiC there. The initial steps around the TSD core in heights of half a unit cell are partly decomposed into smaller steps in heights of 0.25 nm or 0.5 nm after graphene growth.

The Raman features of the EGs on the TSD core and in the area 4 μm away from the core as marked by the circles in Fig. 6(a) are tested respectively. It is observed that the layer numbers of graphene films are larger, i.e., the graphene films are thicker and the crystalline quality is poorer on the hexagonal holes than in the area with a uniform stepped structure, which is supported by the Raman spectra shown in Fig. 6(b). The crystalline quality of the EG in the area far from the TSD core is also of a high quality without a clear *D* peak proved by its Raman spectrum. The above results prove that the defect in SiC is one of the main origins of domain boundaries in EGs. The above results suggest that a high quality SiC substrate is a necessary requirement for fabricating EGs with a high crystalline quality.

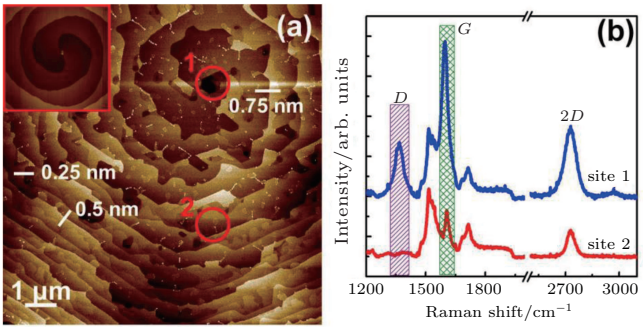


Fig. 6. (color online) AFM morphology of EG on a TSD site of SiC (0001). (b) Raman spectra measured on the sites marked by the circles in panel (a).

4. Conclusions

The influence of defects in SiC (0001) on the quality of EGs is studied and discussed. A higher crystalline quality graphene with better uniformity and larger graphene domain is found on high quality SiC (0001) and compared with those on SiC (0001) with a high defect density. The reasons are in the following. Graphene islands grown in the defective area on SiC (0001) possess different crystalline orientations that result in a domain boundary, while the islands enlarge and encounter. The irregular steps formed in the area of the dislocations contribute to the poor uniformity of the EGs. Meanwhile, the EGs on the defect sites are a little thicker than those in a perfect crystalline area of SiC (0001). Therefore, a high quality SiC is a necessary prerequisite for high quality EGs besides the optimal growth procedure.

References

[1] Morozov S V, Novoselov K S, Katsnelson M I, Schedin F, Elias D C, Jaszczak J A and Geim A K 2008 *Phys. Rev. Lett.* **100** 016602

[2] Geim A K and Novoselov K S 2007 *Nat. Mater.* **6** 183

[3] Zhang Y B, Tan Y W, Stormer H L and Kim P 2005 *Nature* **438** 201

[4] Lin Y M, Jenkins K A, Valdes-Garcia A, Small J P, Farmer D B and Avouris P 2009 *Nano Lett.* **9** 422

[5] Berger C, Song Z M, Li X B, Wu X S, Brown N, Naud C, Mayou D, Li T B, Hass J, Marchenkov A N, Conrad E H, First P N and de Heer W A 2006 *Science* **312** 1191

[6] Dimitrakopoulos C, Lin Y M, Grill A, Farmer D B, Freitag M, Sun Y N, Han S J, Chen Z H, Jenkins K A, Zhu Y, Liu Z H, McArdle T J, Ott J A, Wisnieff R and Avouris P 2010 *J. Vac. Sci. Technol. B* **28** 985

[7] Wang Q Y, Zhang W H, Wang L L, He K, Ma X C and Xue Q K 2013 *J. Phys.: Condens. Matter* **25** 095002

[8] Emtsev K V, Bostwick A, Horn K, Jobst J, Kellogg G L, Ley L, McChesney J L, Ohta T, Reshanov S A, Rohrl J, Rotenberg E, Schmid A K, Waldmann D, Weber H B and Seyller T 2009 *Nat. Mater.* **8** 203

[9] Nyakiti L O, Myers-Ward R L, Wheeler V D, Imhoff E A, Bezares F J, Chun H, Caldwell J D, Friedman A L, Matis B R, Baldwin J W, Campbell P M, Culbertson J C, Eddy C R, Jernigan G G and Gaskill D K 2012 *Nano Lett.* **12** 1749

[10] Jobst J, Waldmann D, Speck F, Hirner R, Maude D K, Seyller T and Weber H B 2011 *Solid State Commun.* **151** 1061

[11] Lin Y M, Valdes-Garcia A, Han S J, Farmer D B, Meric I, Sun Y N, Wu Y Q, Dimitrakopoulos C, Grill A, Avouris P and Jenkins K A 2011 *Science* **332** 1294

[12] First P N, de Heer W A, Seyller T, Berger C, Stroscio J A and Moon J S 2010 *Mater. Bull.* **35** 296

[13] Hass J, de Heer W A and Conrad E H 2008 *J. Phys.: Condens. Matter* **20** 323202

[14] Robinson J, Weng X J, Trumbull K, Cavalero R, Wetherington M, Frantz E, LaBella M, Hughes Z, Fanton M and Snyder D 2010 *ACS Nano* **4** 153

[15] Bolotin K I, Sikes K J, Jiang Z, Klima M, Fudenberg G, Hone J, Kim P and Stormer H L 2008 *Solid State Commun.* **146** 351

[16] Luxmi, Nie S, Fisher P J, Feenstra R M, Gu G and Sun Y G 2009 *J. Electron. Mater.* **38** 718

[17] Bolen M L, Harrison S E, Biedermann L B and Capano M A 2009 *Phys. Rev. B* **80** 115433

[18] Oliveira M H, Schumann T, Ramsteiner M, Lopes J M J and Riechert H 2011 *Appl. Phys. Lett.* **99** 111901

[19] Borovikov V and Zangwill A 2009 *Phys. Rev. B* **80** 121406

[20] Hannon J B and Tromp R M 2008 *Phys. Rev. B* **77** 241404

[21] Guo Y, Guo L W, Huang J, Yang R, Jia Y P, Lin J J, Lu W, Li Z L and Chen X L 2014 *J. Appl. Phys.* **115** 043527

[22] Cancado L G, Takai K, Enoki T, Endo M, Kim Y A, Mizusaki H, Jorio A, Coelho L N, Magalhaes-Paniago R and Pimenta M A 2006 *Appl. Phys. Lett.* **88** 163106

[23] Cancado L G, Jorio A, Ferreira E H M, Stavale F, Achete C A, Capaz R B, Moutinho M V O, Lombardo A, Kulmala T S and Ferrari A C 2011 *Nano Lett.* **11** 3190

[24] Ni Z, Chen W, Fan X, Kuo J, Yu T, Wee A and Shen Z 2008 *Phys. Rev. B* **77** 115416

[25] Ni Z, Wang Y, Yu T and Shen Z 2010 *Nano Res.* **1** 273

[26] Graf D, Molitor F, Ensslin K, Stampfer C, Jungen A, Hierold C and Wirtz L 2007 *Nano Lett.* **7** 238

[27] Ni Z H, Wang H M, Kasim J, Fan H M, Yu T, Wu Y H, Feng Y P and Shen Z X 2007 *Nano Lett.* **7** 2758

[28] Wang Y Y, Ni Z H, Shen Z X, Wang H M and Wu Y H 2008 *Appl. Phys. Lett.* **92** 043121

[29] Zhuang D and Edgar J H 2005 *Mater. Sci. & Eng. R-Reports* **48** 1

[30] Yang R, Shi Z W, Zhang L C, Shi D X and Zhang G Y 2011 *Nano Lett.* **11** 4083

[31] Vanbommel A J, Crombeen J E and Vantooren A 1975 *Surf. Sci.* **48** 463